Anomalous magnetic phase diagrams in the site-diluted Heisenberg antiferromagnets, $A_2Fe_{1-x}In_xCl_5.H_2O$ (A = Rb, K)

1999 J. Phys.: Condens. Matter 11 4409

(http://iopscience.iop.org/0953-8984/11/22/312)

J. Phys.: Condens. Matter **11** (1999) 4409–4425. Printed in the UK PII: S0953-8984(99)99566-8

Anomalous magnetic phase diagrams in the site-diluted Heisenberg antiferromagnets, $A_2Fe_{1-x}In_xCl_5{\cdot}H_2O$ (A = Rb, K)

Javier Campo†, Fernando Palacio†, M Carmen Morón†, Carlos C Becerra‡ and Armando Paduan-Filho‡

† Instituto de Ciencia de Materiales de Aragón, CSIC–Universidad de Zaragoza, 50009 Zaragoza, Spain

‡ Instituto de Fisica, Universidade de São Paulo, CP 66318, CEP 05315-970, São Paulo, Brazil

Received 23 November 1998, in final form 22 February 1999

Abstract. The effect of the substitution of diamagnetic ions for paramagnetic ones in the magnetic phase diagrams of the low-anisotropy antiferromagnets $A_2Fe_{1-x}In_xCl_5{\cdot}H_2O$ (A = Rb, K) is investigated. In the region where the spin-flop (SF) transition occurs, the consequences of dilution are manifested as the appearance of a structure of secondary transition lines and a substantial enhancement of the transition width. In the SF region a multiple-peak structure is observed in the ac susceptibility measurements which is associated with the secondary transition lines. This behaviour is discussed in terms of several mechanisms proposed previously. When the sample is cooled in applied fields below $H_{SF}(T)$ we observe the presence of a remanent magnetization (M_r) in the antiferromagnetic (AF) phase. Such magnetization was previously found in these solid solutions at very low fields (a few Oe). Here we also find that M_r follows a temperature dependence that is independent of the concentration x and is the same for the K and Rb derivatives.

1. Introduction

The problem of magnetic disorder and its role in critical phenomena has received considerable attention in the literature. In particular the behaviour of a diluted uniaxial antiferromagnet in a field applied along the axis of easy magnetization has been explored in the region of applied fields where a spin-flop (SF) transition occurs in the undiluted system.

Pulsed-field experiments on the *large-anisotropy* diluted antiferromagnet $Fe_{1-x}Zn_xF_2$ [1] indicate that at low temperature single-spin 'exchange flips' could occur, the transition to the transverse spin-flop alignment being very wide and accompanied with hysteresis in dM/dH. The effects of disorder in the SF region of the magnetic phase diagram of the *low-anisotropy* antiferromagnets have been already investigated for $Mn_{1-x}Zn_xF_2$, $K_2Fe(Cl_{1-x}Br_x)_5{\cdot}H_2O$ and $K_2Fe_{1-x}In_xCl_5{\cdot}H_2O$ [2–9]. For $Mn_{1-x}Zn_xF_2$, anomalies were observed in the SF phase boundary, $H_{SF}(T)$, near the bicritical point (BCP) [7, 8]. Cowley *et al* [10], analysing neutron critical scattering data, found a double boundary line that delimits a region where a kind of mixed phase could exist between the antiferromagnetic (AF) and the SF regions. In diluted $K_2Fe(Cl_{1-x}Br_x)_5{\cdot}H_2O$ and $K_2Fe_{1-x}In_xCl_5{\cdot}H_2O$ compounds, hysteresis effects have been observed in $H_{SF}(T)$ line accompanied by an anomalous enhancement of the transition width [5, 6]. A similar enhancement but without hysteresis has also been observed for $(K_{1-x}Rb_x)_2FeCl_5{\cdot}H_2O$ solid solutions [2]. An anomalously large SF transition region

0953-8984/99/224409+17$19.50

accompanied with hysteresis was also observed for the low-anisotropy diluted antiferromagnet $K_2Fe_{1-x}In_xCl_5{\cdot}H_2O$ [2, 5, 6]. A very broad SF transition has also been observed for the randomly mixed antiferromagnet $Fe_xMn_{1-x}F_2$ [11]. In this case, for small values of x, mean-field calculations show that a canted intermediate phase in which the spins rotate continuously between the AF and the SF phase over this wide transition region may be present. The enhanced width has also been attributed to the existence of an induced intermediate phase in $CoBr_2 6{\cdot}(0.48D_2O, 0.52H_2O)$ [12].

In this paper we explore the influence of disorder in the magnetic phase diagram of low-anisotropy antiferromagnetic systems in an applied external field in two very different regions: at low applied fields (below 1000 Oe) and at fields of several kOe. At low field we investigate the recently found remanent magnetization in these diluted compounds, which seems to exhibit a kind of universal behaviour. At higher fields (above 10 kOe) we study the behaviour of these systems in the field region were the AF phase becomes unstable and the system is driven to a spin configuration that is transverse to the applied external field.

In the domain of very low applied fields, remanent magnetization was found in all of these diluted low-anisotropy antiferromagnets, $A_2Fe_{1-x}In_xX_5{\cdot}H_2O$ (A = Rb, K and X = Cl, Br) and $Mn_{1-x}Zn_xF_2$ [13–17]. In these works it was shown that if appropriate reduced variables are chosen it is possible to collapse all of the very low-field data on the remanent magnetization of these compounds, with different degrees of dilution and with different crystallographic structures, onto a single universal magnetization curve.

The $A_2Fe_{1-x}In_xCl_5{\cdot}H_2O$ (A = Rb, K) compounds (hereafter referred to, respectively, as Rb–Fe/In and K–Fe/In for simplicity) are solid solutions of the isostructural series $A_2FeCl_5{\cdot}H_2O$ and $A_2InCl_5{\cdot}H_2O$, where A = Rb, K, Cs, NH_4 [18–20]. The magnetic properties of the undiluted compounds have been studied before [18, 21–24] and they can be described using a 3d Heisenberg AF model with the a-axis being the axis of antiferromagnetic alignment. The thermodynamic parameters for these compounds are as follows: $K_2FeCl_5{\cdot}H_2O$ orders at $T_N = 14.06$ K, and the bicritical point occurs at $T_B = 13.9$ K and at a magnetic field of $H_B \approx 29$ kOe; the transition to the SF phase occurs at $H_{SF} = 27.6$ kOe for T close to zero. Its anisotropy-to-exchange ratio is $\alpha = H_A/H_E = 8.5 \times 10^{-3}$. The corresponding parameters for $Rb_2FeCl_5{\cdot}H_2O$ are $T_N = 10.02$ K, $T_B = 9.9$ K, $H_B \approx 18$ kOe, $H_{SF} = 16.2$ kOe and $\alpha = 3.4 \times 10^{-3}$.

2. Experimental procedure

Single crystals of the diluted compounds $A_2Fe_{1-x}In_xCl_5{\cdot}H_2O$ (A = Rb, K) were grown from aqueous solutions of ACl, $InCl_3$ and $FeCl_3{\cdot}6H_2O$ in an acid environment [25]. The size of the crystals selected for this work was $3 \times 3 \times 3$ mm^3, approximately. The In contents were determined by means of high-temperature magnetic susceptibility in the temperature region where the compounds follow the Curie–Weiss law. The Curie constant C determined in this procedure is proportional to the content of Fe^{3+} present in a sample. The estimated accuracy of this method is 5%. The results were confirmed by optical absorption spectroscopy carried out on some thin single crystals. The homogeneity of the diluted samples was checked by x-ray fluorescence microanalysis (SEM) of several crystals. The volume probed in each process was 2 μm^3 and for each crystal several regions were examined. The results confirm the existence of a unique phase with a unique indium concentration within the experimental resolution. This also agrees with the x-values determined by $\chi(T)$ experiments: no differences in the value of x were observed between crystals extracted at the same time from the same solution or between pieces cut from a large crystal.

The compositions of the crystal samples used in the magnetic studies were $x = 0.08, 0.10$

and 0.15 for the $Rb_2Fe_{1-x}In_xCl_5{\cdot}H_2O$ compounds and $x = 0.15$ for the $K_2Fe_{1-x}In_xCl_5{\cdot}H_2O$ compound. Single crystals of Rb–Fe/In, with $x = 0.0$, 0.08, 0.15, 0.27, 0.47, 0.68, 0.86 and 1.0, were also grown and then crushed to powder for use in the x-ray diffraction experiments.

Magnetic ac susceptibility and magnetization measurements were carried out using a SQUID magnetometer, MPMSR2, manufactured by Quantum Design. The frequency and excitation amplitude used in the ac magnetic susceptibility measurements were 10 Hz and 4.5 Oe, respectively. Magnetic fields up to 5 T were applied using the built-in superconducting coil, the accuracy being better than 10 Oe over the entire interval. Magnetic field-dependent measurements were performed with the superconducting coil in the permanent regime; i.e. for each point the coil was disconnected from the current source. In this mode a better stabilization of the magnetic field is achieved and the signal-to-noise ratio is improved. The temperature was controlled by means of a carbon glass resistance thermometer placed close to the sample holder. The temperature deviation was maintained within 0.1%, the minimum achievable using this equipment.

The crystals were carefully oriented, with their axis of antiferromagnetic alignment (the a-axis for all of the crystals) parallel to the direction of the magnetic field. Given the external morphology of the crystals [26] a visual orientation of the crystals in the sample holder is easy. In several cases however, the orientation was checked by means of the x-ray Laue technique. A minor misorientation (of the order of 0.5° to 1°) of this crystal axis with respect to the axial field can prevent the appearance of a first-order-line $H_{SF}(T)$ boundary at the spin-flop transition. This requirement becomes increasingly exigent as the temperature approaches the bicritical point [27]. Since all crystals studied here are of about the same shape and size, their demagnetization factors were considered to be the same.

In some experiments the sample was initially cooled to the lowest temperature in the absence of an applied magnetic field. Subsequently, at this lowest temperature, a field H was applied along the easy axis and the measurements were taken while warming the sample in this field. We call this procedure field heating after zero-field cooling (FHAZFC) instead of using the term ZFC common in the literature. Another procedure consists in cooling the sample through the transition in an applied field H. We refer to this field-cooling procedure by its usual acronym, FC.

X-ray powder diffractograms used for the determination of the unit-cell parameters of the $Rb_2Fe_{1-x}In_xCl_5{\cdot}H_2O$ ($0 \leqslant x \leqslant 1$) series were recorder on a back-monochromatized Cu Kα Rigaku diffractometer. The data were collected at 2θ-values between 18 and 90 degrees with a step size of 0.02°.

3. Results

3.1. Behaviour in the low-field region

Figures 1 and 2 show the dc susceptibility $\chi_{DC} = M/H$ versus temperature measured in different applied magnetic fields ranging from 0.15 kOe to 40 kOe for the Rb–Fe/In sample with $x = 0.15$ and from 1 kOe to 29.5 kOe for the K–Fe/In sample with $x = 0.15$. The samples of Rb–Fe/In with $x = 0.08$ and 0.10 exhibit a similar behaviour. The data shown in figures 1(a), 2(a), 2(b) also show the results of FHAZFC–FC cycles for the applied magnetic fields shown in the figures. The experimental procedure for these kinds of cycle has been discussed in the previous section.

The data in figure 1(a) for the Rb–Fe/In system show that, for magnetic fields below 1000 Oe, χ_{DC} increases as temperature decreases. A similar behaviour is observed for the K–Fe/In derivative (figure 2(a)). At higher magnetic fields this trend changes and χ_{DC}

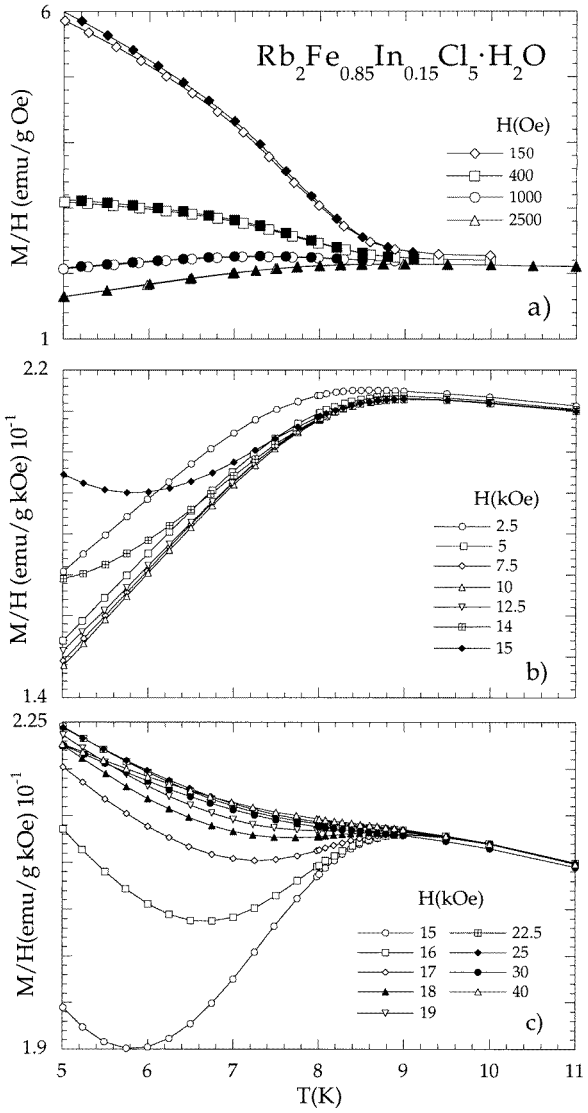

Figure 1. The temperature dependence of the magnetization in $Rb_2Fe_{0.85}In_{0.15}Cl_5{\cdot}H_2O$ at different constant magnetic fields: (a) $150 \leqslant H \leqslant 2500$ Oe, (b) $2.5 \leqslant H \leqslant 15$ kOe, (c) $15 \leqslant H \leqslant 40$ kOe. Full and open symbols refer, respectively, to FC and FHAZFC measurements.

decreases below T_N because the contribution to the magnetization of the parallel susceptibility $\chi_{\parallel}H$ tends to zero as T decreases (see figures 2(a) and 2(b)). At applied magnetic fields higher than 10 kOe for the Rb–Fe/In compounds and 25 kOe for the K–Fe/In compounds the susceptibility $\chi_{DC}(T)$ tends to increase due to the proximity of the AF–SF phase boundary. As the magnetic field continues to increase, a temperature $T < T_N$ is reached at which the system enters into the SF phase. This is illustrated in figures 1(b) and 1(c) for fields between 14 and 18 kOe for the Rb–Fe/In samples and in figure 2(b) by the curves above 27 kOe for the K–Fe/In samples. This phase transition is marked by an increment in the magnetization associated with

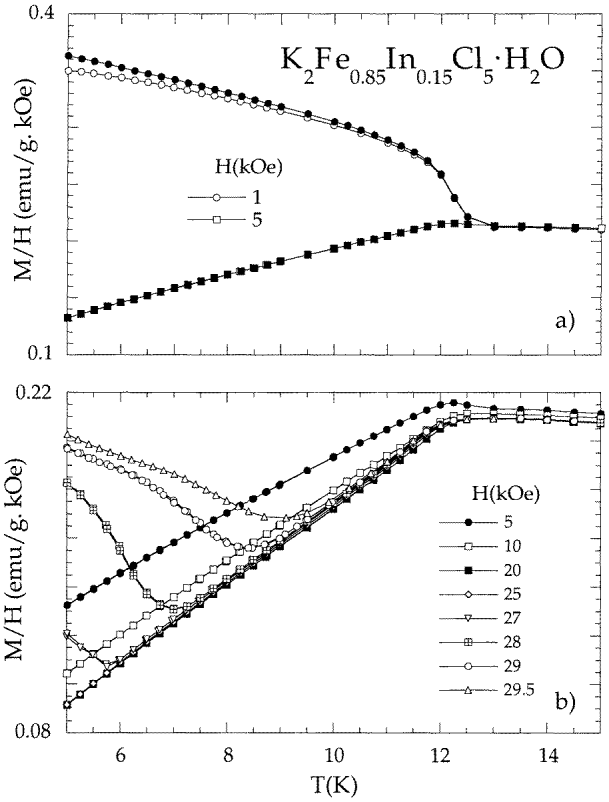

Figure 2. The temperature dependence of the magnetization in $K_2Fe_{0.85}In_{0.15}Cl_5 \cdot H_2O$ at different constant magnetic fields: (a) $1 \leqslant H \leqslant 5$ kOe, (b) $5 \leqslant H \leqslant 29.5$ kOe. Full and open symbols refer, respectively, to FC and FHAZFC measurements.

the change from the AF to the SF phase. That is, the susceptibility increases as the system changes from a parallel alignment to a transverse one. Above 18 kOe the Rb–Fe/In system changes directly from the paramagnetic phase to the SF phase with decreasing temperature. This is shown in figure 1(c).

The FHAZFC–FC cycles show that an irreversibility is observed for magnetic fields of 150 and 400 Oe for Rb–Fe/In derivatives (figure 1(a)) and of 1 kOe for K–Fe/In derivatives (figure 2(a)). These types of cycle were studied in the region of very low fields for $K_2Fe_{0.97}In_{0.03}Cl_5 \cdot H_2O$ [13, 28].

The magnetization for an antiferromagnet is expected to increase linearly with the magnetic field for $T < T_N$ and $H \ll H_{SF}(T)$. Here however an excess of magnetization, M_r, is observed at low magnetic fields. It is evident in the increment of the dc susceptibility shown in figures 1(a) and 2(a).

As H increases, the $\chi_\parallel H$-term becomes very large compared to M_r; M and $\chi_\parallel H$ are nearly equal and this prevents one from extracting an accurate value of M_r. The values of M_r (calculated after subtracting $\chi_\parallel H$ from the experimental values of M) can be normalized to 1 at 5 K for all cooling fields. The temperature dependence of such a reduced M_r is shown in figure 3. We can see that all of these curves follow approximately the same temperature behaviour.

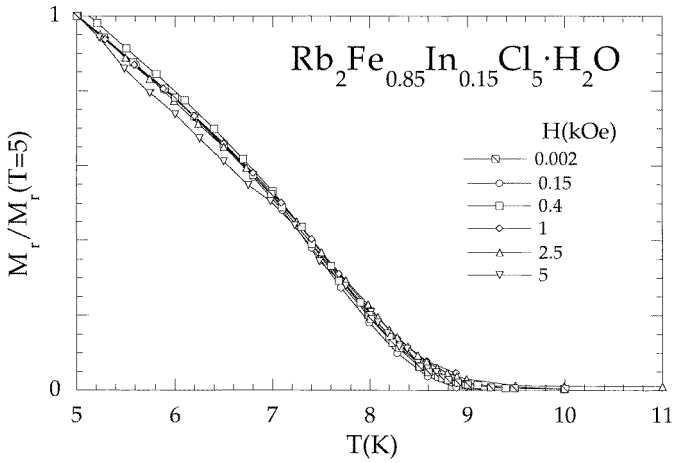

Figure 3. Normalized $M_r(T)/M_r$ ($T = 5$ K) as a function of T for $Rb_2Fe_{0.85}In_{0.15}Cl_5{\cdot}H_2O$.

3.2. Secondary peak structure and enhanced width in the spin-flop region

The isothermal ac susceptibility has been measured as a function of the magnetic field for all of the samples studied in this work. In figure 4 these curves are shown for the Rb–Fe/In compound with $x = 0.10$, for temperatures between 5 K and 9.75 K. We observe a structure formed by an intense principal peak and several, less intense, secondary peaks located at higher magnetic fields. As the temperature increases these secondary peaks become less well resolved. The out-of-phase component, $\chi''(H)$, shows the same peak structure. The same behaviour is observed for the Rb–Fe/In sample with $x = 0.08$. The experiments were repeated with samples grown from the same batch, and consistent results were obtained. The distance between two consecutive peaks is independent of the temperature and approximately the same for the Rb–Fe/In compounds with $x = 0.08$ and $x = 0.10$. An analysis of the positions of the

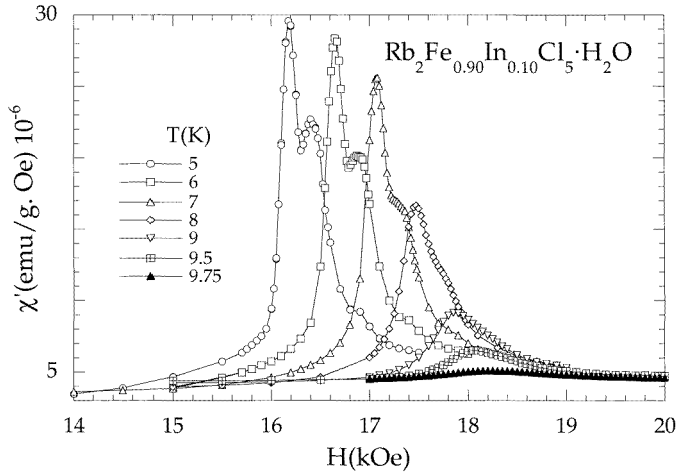

Figure 4. Isothermal ac susceptibility (χ) versus magnetic field (H) in the region of the AF–SF transition for $Rb_2Fe_{0.90}In_{0.10}Cl_5{\cdot}H_2O$.

peaks in these isothermal susceptibility curves indicates that the position and the full width at half-maximum (FWHM) for the principal peak (200 Oe) are nearly the same as those for the SF peak of the same isotherm measured for the undiluted compound. As T increases, the positions of the principal and secondary peaks are shifted towards higher magnetic fields and the width of each peak increases.

The ac susceptibility–temperature curves at constant magnetic field (17.7 kOe $\leqslant H \leqslant$ 18.6 kOe), $\chi_{ac}(T)$, are shown in figure 5 for the Rb–Fe/In compound with $x = 0.08$. Here we observe a behaviour in the SF region that is consistent with that found for the $\chi_{ac}(H)$ curves shown in figure 4. As T decreases, a large peak appears in $\chi_{ac}(T)$ that is related to the principal peak in $\chi_{ac}(H)$. At lower temperatures, other peaks appear which are associated with the secondary peak structure. The AF–P transition is barely visible in this figure and it is located at the lower right of the curves.

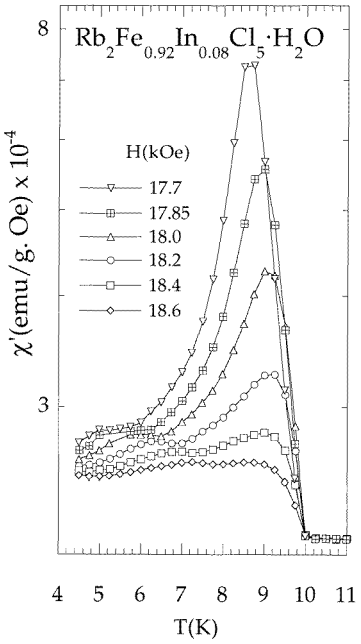

Figure 5. Alternating-current susceptibility (χ) versus temperature (T) in the region of the AF–SF transition for $Rb_2Fe_{0.92}In_{0.08}Cl_5{\cdot}H_2O$ at different constant magnetic fields.

Susceptibility isotherms for the Rb–Fe/In sample with $x = 0.15$ are shown in figure 6. For this sample the principal and secondary peak structure merge into a unique peak with an anomalous width (FWHM = 2000 Oe). For each temperature, this peak is shifted towards lower magnetic fields when compared with the corresponding data for samples with $x = 0.08$ and 0.10 and the undiluted compound. As T increases, the position of the peak moves to higher magnetic fields. The isothermal χ–H runs were carried out for both increasing and decreasing field. The results were completely reversible and no hysteresis effects were found for the Rb–Fe/In crystal.

Figure 7 shows the field dependence of the ac susceptibility and magnetization data obtained at 5 K for a sample of K–Fe/In with $x = 0.15$. An irreversibility is observed for the magnetization curves obtained with increasing and decreasing field. This small magnetic hysteresis occurs in the region where M changes more rapidly with H in the transition towards

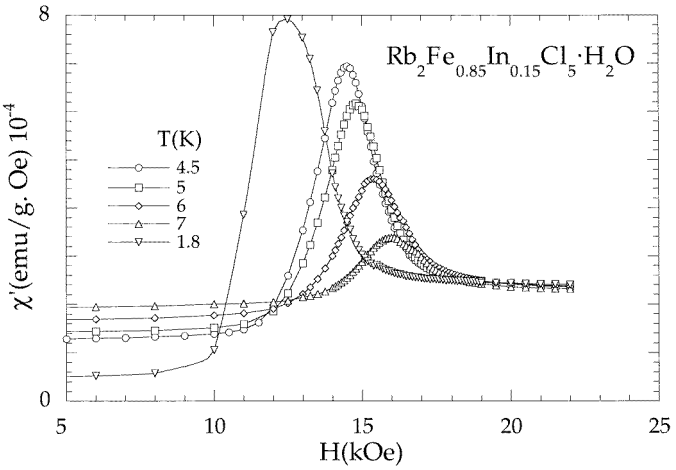

Figure 6. Isothermal ac susceptibility (χ) versus magnetic field (H) in the region of the AF–SF transition for $Rb_2Fe_{0.85}In_{0.15}Cl_5{\cdot}H_2O$.

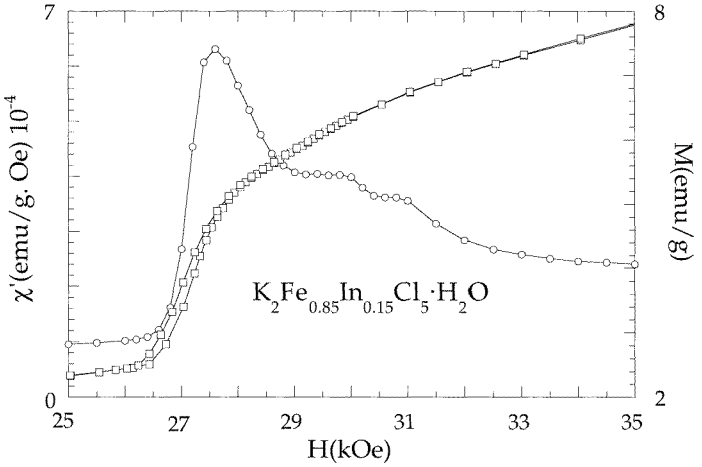

Figure 7. Alternating-current susceptibility (χ) versus magnetic field (H) (circles) and magnetization (M) versus magnetic field (H) (squares) in the region of the AF–SF transition for $K_2Fe_{0.85}In_{0.15}Cl_5{\cdot}H_2O$ at $T = 5$ K. The magnetization curve shows a small hysteresis for increasing and decreasing H.

(or from) the SF phase. The slope of the M–H curve changes continuously until it stabilizes when the SF phase is reached. For this sample the hysteresis width decreases from 200 Oe at $T = 5$ K to an almost negligible value at $T = 8$ K. The isothermal ac susceptibility curve shown in the same figure exhibits a similar behaviour to that observed for the Rb–Fe/In samples with $x = 0.08$ and $x = 0.10$. As for Rb–Fe/In with $x = 0.15$, the principal peak appears at a lower magnetic fields than for the undiluted $K_2FeCl_5{\cdot}H_2O$ compound. The secondary peak structure in the $\chi'(H)$ curves, as illustrated in figure 7, reflects the slope changes in the isothermal magnetization curve.

The principal results obtained can be summarized as follows: for the two Rb–Fe/In and K–Fe/In samples with $x = 0.15$, the width of the SF transition is anomalously large and, in both

cases, the $H_{SF}(T)$ line occurs at fields lower than in the case of the non-diluted compounds. For the $x = 0.08$ and $x = 0.10$ Rb–Fe/In samples, the principal $H_{SF}(T)$ line of peaks occurs at nearly the same $H_{SF}(T)$ fields as for the pure compounds. Moreover, a secondary peak structure is observed for the samples of Rb–Fe/In with $x = 0.08$ and $x = 0.10$ and of K–Fe/In with $x = 0.15$. No hysteresis in the $M(H)$ isothermal curves was observed for any of the diluted Rb compounds investigated.

3.3. Magnetic phase diagrams (MPD)

Figure 8 shows the magnetic phase diagram of the $Rb_2Fe_{1-x}In_xCl_5{\cdot}H_2O$ compound with $x = 0.08$. The boundary lines have been obtained from the $M(H)$ and $\chi'(H)$ curves at constant temperature and from $M(T)$ and $\chi'(T)$ curves at constant applied field. The $T_C^{\parallel,\perp}(H)$ boundaries have been determined from the magnetization–temperature curves and also from points where $T\,\mathrm{d}\chi(T)/\mathrm{d}T$ versus T shows a maximum. The spin-flop boundary line, $H_{SF}(T)$, was taken as the locus $[T, H]$ for which the $\chi'(H)$ curves have a maximum. Interestingly, several lines can, in fact, be distinguished in this case as can be clearly seen in the inset of figure 8. The difference in field between consecutive lines that is observed in the inset suggests that successive lines in this region are equally spaced. The lower line occurs approximately at the position where the $H_{SF}(T)$ line occurs in the MPD of the undiluted Rb compound. These lines join the phase boundaries to the paramagnetic phase, $T_C^{\parallel,\perp}(H)$, at the point $[T, H] = [9.8 \pm 0.1\ \mathrm{K}, 18.1 \pm 0.1\ \mathrm{kOe}]$. This point is rather close to the bicritical point for $Rb_2FeCl_5{\cdot}H_2O$. The MPD obtained for the $x = 0.10$ Rb derivative (not shown) shows the same behaviour. In table 1 the Néel temperatures T_N (K), bicritical temperatures T_B (K) and bicritical fields H_B (kOe) for the dilutions studied in this work are summarized.

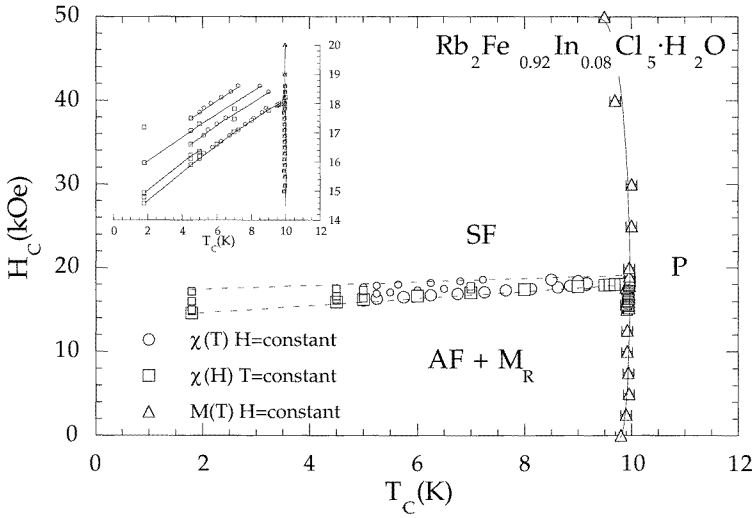

Figure 8. The magnetic phase diagram (MPD) of $Rb_2Fe_{0.92}In_{0.08}Cl_5{\cdot}H_2O$. The inset shows a zoom of the AF–SF transition region. The points on this diagram have been calculated from $\chi(T)$, $\chi(H)$ and $M(T)$ measurements at, respectively, constant H, constant T and constant H.

Figure 9 represents the MPD found for the Rb–Fe/In sample with $x = 0.15$. The main difference with respect to the MPD of the $x = 0.08$ and 0.10 Rb–Fe/In compounds is that in the high-field region we observe a single critical $H_{SF}(T)$ boundary line at fields lower than the boundary line for pure $Rb_2FeCl_5{\cdot}H_2O$.

Table 1. Summary of the anisotropy parameters $\alpha = H_A/H_E$, Néel temperatures T_N(K), bicritical temperatures T_B (K) and bicritical fields H_B (kOe) for $A_2Fe_{1-x}In_xCl_5{\cdot}H_2O$ (A = Rb, K).

Sample	$\alpha = H_A/H_E$	T_N (K)	T_B (K)	H_B (kOe)
$K_2FeCl_5{\cdot}H_2O$	8.5×10^{-3}	14.06	13.6	34.1
$Rb_2FeCl_5{\cdot}H_2O$	3.4×10^{-3}	10.02 ± 0.05	9.96 ± 0.05	18.18 ± 0.05
$Rb_2Fe_{0.92}In_{0.08}Cl_5{\cdot}H_2O$		9.9 ± 0.1	9.8 ± 0.1	18.1 ± 0.1
$Rb_2Fe_{0.90}In_{0.10}Cl_5{\cdot}H_2O$		9.75 ± 0.1	9.6 ± 0.1	18.5 ± 0.5
$Rb_2Fe_{0.85}In_{0.15}Cl_5{\cdot}H_2O$		8.75 ± 0.1	8.2 ± 0.1	17.4 ± 0.05
$K_2Fe_{0.85}In_{0.15}Cl_5{\cdot}H_2O$		12.6 ± 0.1	11.2 ± 0.1	31 ± 0.1

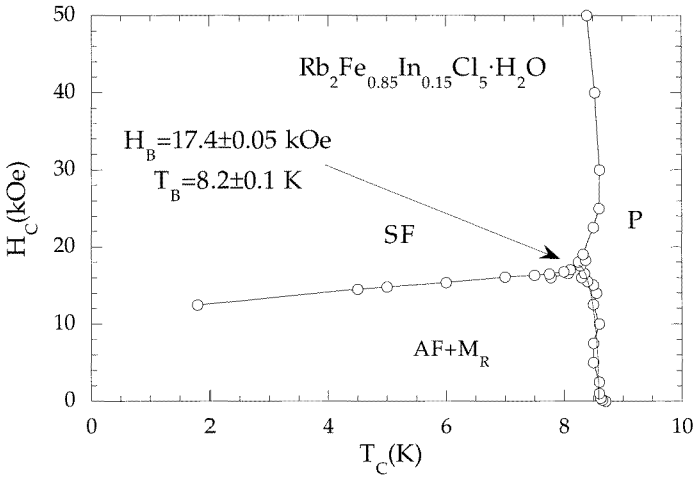

Figure 9. The magnetic phase diagram (MPD) of $Rb_2Fe_{0.85}In_{0.15}Cl_5{\cdot}H_2O$. The H_{SF}-line is located slightly lower than the same line for the undiluted compound. In the AF phase we can distinguish two regions depending on the reversibility of the FHAZFC–FC cycles.

The MPD of the $x = 0.15$ K–Fe/In compound, represented in figure 10, also shows in the SF region a secondary peak structure with several lines around the stability limit of the AF–SF phase.

4. Discussion

The very low-field region of the magnetic phase diagram has been extensively studied before [13–17, 28–31] and we refer the reader to the earlier papers for a detailed account of the origin of the observed remanent magnetization mechanisms and of its universal behaviour. The results previously given in this paper indicate that the remanent magnetization is still present if the sample is cooled in a higher field provided that this field is below the $H_{SF}(T)$ phase boundary. For fields above 1 kOe the remanent magnetization is masked by the contribution of the $\chi_{\parallel}H$-term to M. The data collapse of M_r versus T shown in figure 3 is consistent with the behaviour previously found in the above-cited papers.

The second point arising in our experiments is related to the dependence of the position of the principal peak observed in the SF transition region with the impurity contents and also to the origin of the secondary peak structure. For a given value of the exchange interaction, the magnetic field at which the spin-flop transition arises is related to the anisotropy in the

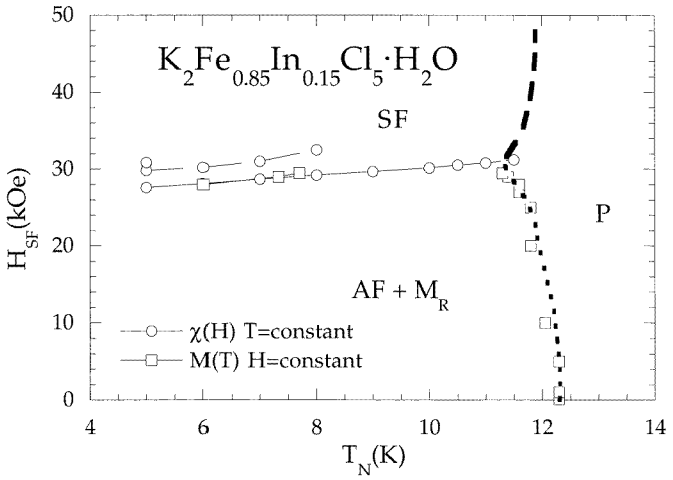

Figure 10. The magnetic phase diagram (MPD) of $K_2Fe_{0.85}In_{0.15}Cl_5{\cdot}H_2O$. The points in this diagram have been calculated from $\chi(H)$ and $M(T)$ measurements at, respectively, constant T and constant H.

crystal through $H_{SF} = (2H_AH_E - H_A^2)^{1/2}$. In our experiments on the Rb–Fe/In samples we observe that for In concentrations of $x = 0.08$ and 0.10 the position of the principal peak is essentially the same as for the undiluted compound while for $x = 0.15$ the peak position is shifted towards lower magnetic fields. If we assume that the principal peak marks the onset of the transition from antiferromagnetic to the transverse spin-flop alignment and that the Néel temperature, which is proportional to H_E, is slightly lower for the diluted compounds, then we can infer that for $x = 0.08$ and 0.10 we have a small increase in the anisotropy. A simple mean-field estimate indicates that a reduction of 1.25 K in the ordering temperature of the Rb–Fe/In $x = 0.15$ sample with respect to the undiluted Rb sample corresponds to a 13% reduction in H_E. This reduction in H_E will be responsible for a 6.5% reduction in H_{SF}. Since the reduction in H_{SF} is 15%, the difference must be supplied by a decrease in the anisotropy field H_A. Thus, for the $x = 0.15$ Rb–Fe/In sample the anisotropy tends to decrease.

Earlier work on the mechanisms responsible for the single-ion anisotropy in the pure compounds of this series indicates that the anisotropy is mainly due to the deformation of the coordination octahedron around each Fe^{3+} ion. These octahedra are each formed by five chlorine ions and one water oxygen ion [18]. Figure 11 shows the unit cell of $A_2FeCl_5{\cdot}H_2O$ in a polyhedral representation.

As the In^{3+} ion is larger than the Fe^{3+} one, the size of the coordination octahedron around In^{3+} is bigger and therefore it should occupy a larger volume in the unit cell. At this point, we can think that the extra volume needed to host the In^{3+} ion is obtained either from a deformation of nearest-neighbour coordination octahedra or from the expansion of lattice constants, which is equivalent to an increase in the unit-cell volume. Both mechanisms are plausible, and a competition between these processes could arise. The first mechanism would increase the anisotropy because it would deform the octahedral environment of the Fe^{3+} ions, thus decreasing the crystal-field symmetry. This in principle would increase $H_{SF}(T)$. In contrast, the unit-cell expansion effect would cause a decrease in the exchange parameter and in the anisotropy of the Fe^{3+} ions. This, therefore, would imply a decrease of $H_{SF}(T)$.

The structural data available in the literature for the undiluted members of the $A_2FeCl_5{\cdot}H_2O$ (A = Rb, K) series show that the Fe–Cl distances are practically the same in

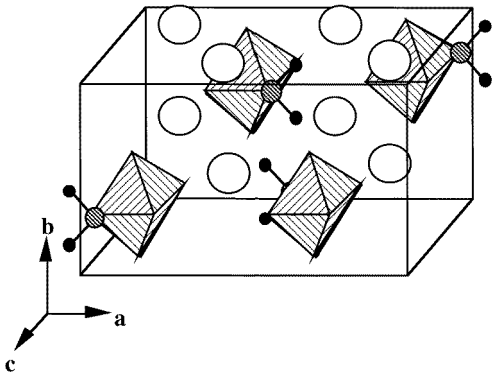

Figure 11. A polyhedral representation of the unit cell of the $A_2FeCl_5{\cdot}H_2O$ (A = Rb, K) family. The Fe^{3+} is surrounded by five Cl and by one O forming an octahedron. The cations A^+ and the hydrogens are represented in the figure by, respectively, large (white) and small (dark) spheres.

the Rb and in the K derivatives (the average Fe–Cl distances are 2.369 Å in the Rb derivatives and 2.362 Å in the K derivatives), while the Fe–O distances are different, being larger in the Rb compound (2.133 Å) than in the K one (2.078 Å) [16, 19, 24]. As a consequence, the octahedral distortion is more accentuated in the K than in the Rb compound. This tendency is accompanied by the decrease in the anisotropy in the Rb compound and also by an increase of the unit-cell volume. Thus, both H_{SF} and T_N, which are related to the overall Fe–Fe distance, decrease.

The model that we propose to explain the change in anisotropy, as a function of the In^{3+} content, is closely related to these effects. We suppose that when the In^{3+} concentration is smaller than a certain value (smaller than 0.15), the distortion of the coordination octahedra dominates over the lattice expansion effect and a small increase in the anisotropy occurs. As the In^{3+} concentration increases the competition between the distortion and the volume increase leads to an expansion of the unit cell which tends to decrease the anisotropy.

In this scenario, the small decrease in T_N for $x = 0.08$ and $x = 0.1$ can be attributed to the distortion of the octahedral environment of the Fe^{3+} ion occurring without any significant change in the Fe^{3+}–Fe^{3+} distance (the Néel temperature is closely related to the Fe^{3+}–Fe^{3+} distance through the Fe–Cl$\cdots$Cl–Fe and Fe–O–H$\cdots$Cl–Fe superexchange constants). For the sample with $x = 0.15$, T_N is significantly smaller (by 1.3 K) and this suggests that the overall Fe^{3+}–Fe^{3+} distance increases and the expansion effect is dominant.

The value x for the concentration crossover between these two tendencies, distortion and expansion, can be associated with the concentration for which the probability of finding one cluster of two or more nearest In atoms ($P = 1 - (1 - x)^6$) is equal to the probability of finding one isolated In atom ($P_1 = (1 - x)^6$). A simple calculation for this lattice shows that this occurs when $x_c \approx 0.12$. We suppose that one cluster of two or more nearest-neighbour impurities expands the unit cell. To check this conjecture, we carried out x-ray powder diffraction experiments on $Rb_2Fe_{1-x}In_xCl_5{\cdot}H_2O$ samples with x ranging from 0.00 to 1.0. The orthorhombic unit-cell parameters were calculated for the space group *Pnma* by fitting the profiles of the experimental Bragg peaks to an appropriate pseudo-Voigt function (see figure 12), by using the pattern-matching technique implemented in the Fullprof program [32]. The evolution of the unit-cell volume with the impurity concentration that is obtained is depicted in figure 13. The standard deviation of the calculated *a*-, *b*- and *c*-parameters affects

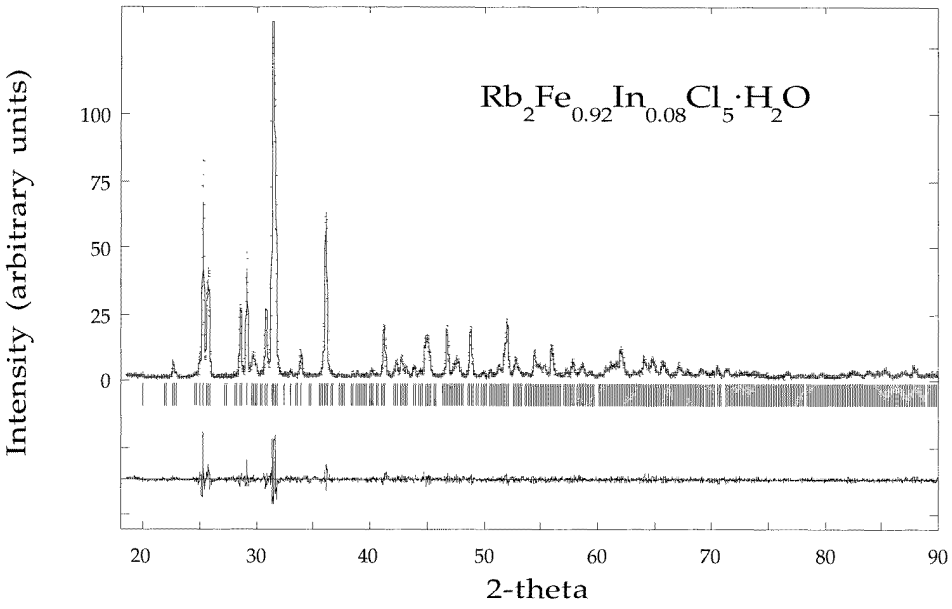

Figure 12. X-ray powder diffractograms of $Rb_2Fe_{0.92}In_{0.08}Cl_5{\cdot}H_2O$ showing the experimental and calculated profiles (see the text for details). The difference pattern is given at the bottom of the figure on the same scale. The angular positions of the allowed Bragg reflections are indicated by small bars.

the fourth decimal places of their values. This seems to confirm the existence of two regimes: at low x, deformation dominates, whereas above $x \approx 0.10$, the unit cell expands.

In the following we will try to explain the origin of the secondary peak structure ($x = 0.08$, 0.10) and the anomalous width of the isothermal susceptibility curves. We can consider three different approaches. First, let us assume an inhomogeneous impurity distribution in the crystal. Strong concentration gradients with dispersion of x around more than a single value can in principle explain the multiple lines at the transition to the transverse phase of the crystal [33]. However, SEM experiments performed on crystals from the same batch as those used in the magnetic measurements have not detected any measurable concentration gradient of In. Moreover, it is observed that secondary peak positions in $x = 0.08$ and 0.10 samples occur at the same values of H for a given temperature (see figure 14), and that the separation between different lines is approximately constant with the value $\Delta H_{SF}(T) = 300 \pm 50$ Oe. If an inhomogeneous impurity distribution is assumed, this result would imply that only certain 'magic' concentration values, always the same, and the value $x = 0.00$ would appear in diluted crystals. This is, in fact, not acceptable.

Another possible approach is based on the ideas of King *et al* [34] about the MPD of anisotropic AF systems. Adapting their ideas to our problem we can suppose that spins could make the transition to the SF phase individually if the applied magnetic field was bigger than the molecular field due to its first neighbours. That is, each magnetic moment would 'see' a local field that depends on the external applied field and the number of nearest neighbours z. This mechanism has been suggested by Shapira *et al* [8] as a possible explanation of an anomalous width of the SF transition of $Mn_{0.75}Zn_{0.25}F_2$. The idea of King *et al* has been generalized by Wong and Cable [35] who consider that a small cluster that consists of N_1 and N_2 spins in sublattices 1 and 2 respectively is linked by a number Q of bonds to the infinite

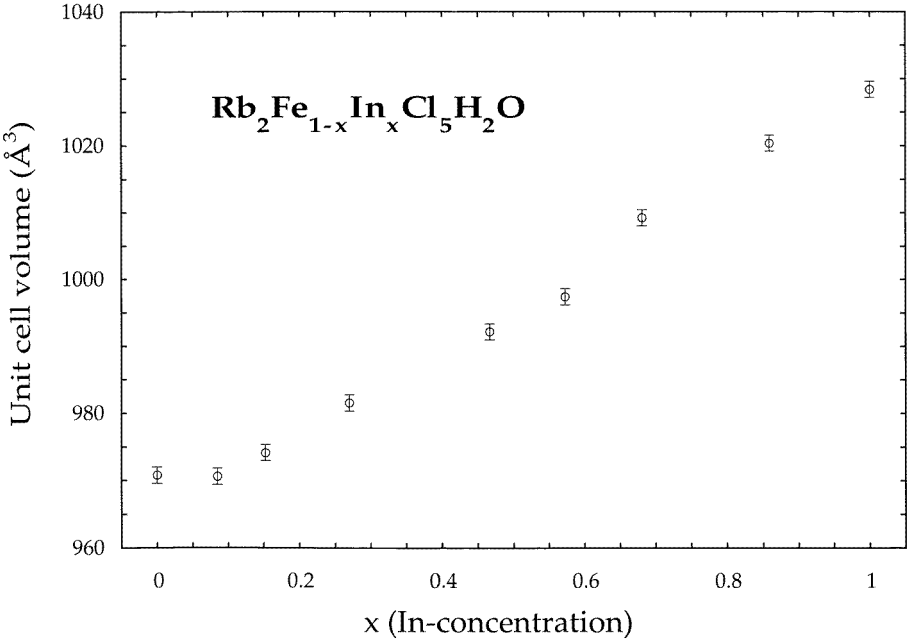

Figure 13. The evolution of the unit-cell volume of the $Rb_2Fe_{1-x}In_xCl_5{\cdot}H_2O$ series with the impurity concentration obtained from x-ray powder diffraction data.

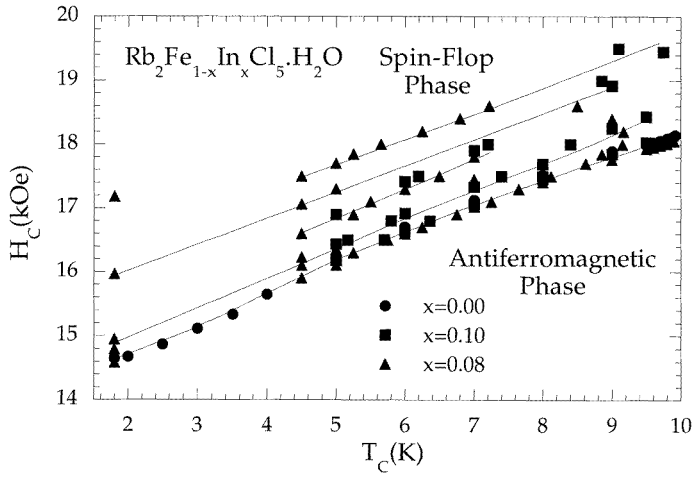

Figure 14. A superposition of the $H_{SF}(T)$ lines determined for the $Rb_2Fe_{1-x}In_xCl_5{\cdot}H_2O$ series with $x = 0$, 0.08, 0.10.

cluster. In this picture, when in the small cluster the Zeeman term due to the external field $Hg\mu_B(N_1 - N_2)S$, is larger than the molecular term $QJ\langle S\rangle S$ (which is created by the infinite cluster), then the small cluster will flip as an independent entity. Each peak observed in $\chi'(H)$ would then reflect the transition of a type of cluster. Two phases would then coexist, one formed by the AF domains and the other one by SF domains. The magnetic field would change their

relative proportions. In this picture, hysteresis would reflect the irreversibility in the domain wall motion. The lack of hysteresis for the Rb–Fe/In samples would be attributable to the weak coercivity of these dilutions. For the K–Fe/In samples, hysteresis is always observed [5, 6]. As the dilution increases, a quasi-continuum local field distribution can arise in the crystal and the secondary peak structure then merges into a unique peak with an enhanced width, as for our $x = 0.15$ Rb–Fe/In sample. On the basis of these ideas, Cowley *et al* [10] suggested the existence of a mixed phase to explain anomalies in the SF transitions of $Mn_{1-x}Zn_xF_2$ dilutions with $x = 0.25$. King *et al* [34] found magnetic hysteresis in the isothermal curves $\chi'(H)$ of $Fe_{1-x}Zn_xF_2$ dilutions, and they also observed an equally spaced series of peaks in these curves. In figure 14 the experimental points for the SF line for $x = 0.00$, and the principal and secondary lines generated by the experimental points obtained for the $x = 0.08$, and 0.10 samples, are represented. We can see that there is a good match for the secondary structures of both diluted compounds, and between the principal line of the diluted compounds and the SF line of the pure system.

In addition, these authors report that there is a magnetic field separating two hysteresis regimes, strong for smaller fields and weak for higher fields. For the K–Fe/In dilutions we find a similar pattern: a region with hysteresis at lower fields and at slightly higher field a lack of detectable hysteresis. The above explanation can at least accommodate some of the features found in our experiments on the Rb–Fe/In and K–Fe/In diluted samples.

The third possibility is related to the Aharony prediction [36] that a new intermediate phase, arising due to random fields (RFs) in a diluted low-anisotropy antiferromagnet, could appear in the vicinity of the bicritical point of the otherwise undiluted system. This phase would be delimited by two second-order lines joining now at a tetracritical point and would be characterized by a gradual rotation of the Néel vector (the difference of the magnetization vectors of sublattice) from a direction parallel to $\boldsymbol{H}$ to a perpendicular one. In our case the anomalous width for the $x = 0.15$ Rb–Fe/In sample might indicate the presence of such an intermediate phase arising from RFs. Anomalously wide SF transitions have been previously cited as evidence of an intermediate phase [12]. Since only the Rb–Fe/In samples show a lack of hysteresis in this region, only this system could in principle meet these requirements.

At this point is difficult to choose between the possibilities of a mixed phase and an intermediate phase in the Rb–Fe/In samples. It has been proposed that neutron scattering experiments could be used to determine the magnetic structure as a function of the magnetic field in the SF region and the origin of the secondary peak structure. Preliminary results of neutron scattering investigations seem to be consistent with the existence of an intermediate phase [3], but more experiments are needed to confirm this result. In any case, for the K–Fe/In samples the intermediate phase seems to be ruled out due to the systematic observation of hysteresis.

5. Conclusions

The substitution of diamagnetic ions for paramagnetic ones in the magnetic phase diagrams of the low-anisotropy antiferromagnetic systems $A_2Fe_{1-x}In_xCl_5{\cdot}H_2O$ (A = Rb, K) leads to the appearance of a secondary peak structure in the region of the phase diagram where a transition from the AF phase to the SF phase occurs. These peaks have been analysed and discussed. In the case of the K–Fe/In compounds the anomalous width of the region of the transition to the transverse phase (the spin-flop phase) and the structure of the peaks observed seem to be consistent with a model in which the transition occurs in a stepwise fashion, with coexistence of the AF phase and phases of transverse alignment. In the case of the Rb-based diluted samples, besides the above mechanism, an intermediate type of phase similar to the one

proposed by Aharony and generated by RFs cannot be ruled out. A mechanism has also been proposed to explain the variation of the anisotropy of the magnetic ions as the concentration of diamagnetic impurities increases, which also explains the small decrease in the zero-field ordering temperature T_N for the Rb–Fe/In samples with dilution $x = 0.08$ and $x = 010$ as compared to the much larger decrease in T_N observed for the $x = 015$ sample. This latter mechanism can also explain the relative positions of the principal peaks observed for the spin-flop transition of the Rb–Fe/In-based samples. We still do not have an explanation for the equally spaced lines of points associated with the secondary peak structure for the Rb–Fe/In diluted samples. Quantitative predictions of this effect are desirable. In the low-field region of the magnetic phase diagram, a remanent magnetization is observed and its behaviour is consistent with that previously found for other diluted low-anisotropy antiferromagnetic systems.

Acknowledgments

Thanks are due to Isabel Mayoral and to Elena Martínez for, respectively, growing the Rb derivative samples with $x = 0.08, 0.10, 0.15$ and for useful technical support in the magnetic experiments. The research at the University of Zaragoza was supported by CICYT grants MAT92-896, MAT94-0043 and MAT97-951. The research at the University of São Paulo was supported by grants from the CNPq and FAPESP, grant numbers 96/12051-1 and 96/06208-5 and by FINEP—Financiadora de Estudos e Projetos and the CNPq-RHAE programme. The cooperation between the University of São Paulo and the University of Zaragoza was supported by the cooperative grants CSIC-CNPq and CCInt-USP. One of us (Javier Campo) acknowledges a doctoral fellowship from the Diputación Foral de Navarra

References

[1] King A R, Jaccarino V, Sakakibara T, Motokawa M and Date M 1983 *J. Magn. Magn. Mater.* **34** 1119
[2] Becerra C C, Paduan-Filho A, Palacio F and Barbeta V B 1993 *J. Appl. Phys.* **73** 1
[3] Campo J, Palacio F, Becerra C C, Paduan-Filho A, Fernández-Díaz M T and Rodríguez-Carvajal J 1996 *Physica* B **234–236** 632
[4] Campo J, Palacio F, Paduan-Filho A and Becerra C C 1995 *J. Magn. Magn. Mater.* **140–144** 1521
[5] Paduan-Filho A, Becerra C C and Palacio F 1991 *Phys. Rev.* B **43** 11 107
[6] Paduan-Filho A, Becerra C C, Westphal C, Gabás M and Palacio F 1992 *J. Magn. Magn. Mater.* **104** 269
[7] Shapira Y and Oliveira N F 1983 *Phys. Rev.* B **27** 4336
[8] Shapira Y, Oliveira N F and Foner S 1984 *Phys. Rev.* B **30** 6639
[9] Shapira Y 1985 *J. Appl. Phys.* **57** 3268
[10] Cowley R A, Shirane G, Yoshizawa H, Uemura Y J and Birgeneau R J 1989 *Z. Phys.* B **75** 303
[11] King A R, Toussaint R M, Jaccarino V, Motokawa M, Sakakibara T and Date M 1984 *J. Appl. Phys.* **55** 2324
[12] Basten J A J, de Jonge W J M and Frikkee E 1980 *Phys. Rev.* B **21** 4090
[13] Becerra C C, Paduan-Filho A, Fries T, Shapira Y and Palacio F 1994 *J. Phys.: Condens. Matter* **6** 5725
[14] Fries T, Shapira Y, Paduan-Filho A, Becerra C C and Palacio F 1993 *J. Phys.: Condens Matter* **5** 8083
[15] Fries T, Shapira Y, Paduan-Filho A, Becerra C C and Palacio F 1993 *J. Phys.: Condens. Matter* **5** L107
[16] Gabás M 1995 *Tesis Doctoral* Universidad de Zaragoza
[17] Palacio F, Gabás M, Campo J, Becerra C C, Paduan-Filho A, Fries T and Shapira Y 1994 *Phys. Scr.* T **55** 163
[18] Carlin R L and Palacio F 1985 *Coord. Chem. Rev.* **65** 141
[19] O'Connor C J, Deaver B S and Sinn E 1979 *J. Chem. Phys.* **70** 5161
[20] Solans X, Moron M C and Palacio F 1988 *Acta Crystallogr.* C **44** 965
[21] Paduan-Filho A, Palacio F and Carlin R L 1978 *J. Physique Lett.* **39** L279
[22] Palacio F, Paduan-Filho A and Carlin R L 1980 *Phys. Rev.* B **21** 296
[23] Puertolas J A, Navarro R, Palacio F, Bartolomé J, González D and Carlin R L 1982 *Phys. Rev.* B **26** 395
[24] Gabás M, Palacio F, Rodríguez-Carvajal J and Visser D 1995 *J. Phys.: Condens. Matter.* **7** 4725

[25] Linke W F 1965 *Solubilities of Inorganic and Metal Organic Compounds I* (Washington, DC: American Chemical Society)
[26] Misra S K and Sharp G R 1977 *J. Chem. Phys.* **66** 4172
[27] Rohrer H and Thomas H 1969 *J. Appl. Phys.* **49** 1025
[28] Becerra C C, Paduan-Filho A, Barbeta V, Palacio F, Campo J and Gabás M 1997 *Phys. Rev.* B **56** 3204
[29] Campo J 1995 *Tesis doctoral* Universidad de Zaragoza
[30] Paduan-Filho A, Becerra C C, Barbeta V B, Shapira Y, Campo J and Palacio F 1995 *J. Magn. Magn. Mater.* **140–144** 1925
[31] Palacio F, Gabás M, Campo J, Becerra C C, Paduan-Filho A and Barbeta V B 1997 *Phys. Rev.* B **56** 3196
[32] Rodríguez-Carvajal J 1993 *Physica* B **192** 5
[33] Megy R 1987 *These Doctorale* Université de Paris Sud
[34] King A R, Jaccarino V, Sakakibara T, Motokawa M and Date M 1981 *Phys. Rev. Lett.* **47** 117
[35] Wong P and Cable J W 1983 *Phys. Rev.* B **28** 5361
[36] Aharony A 1978 *Phys. Rev.* B **18** 3328